

Cross-ionization of gas in AGN companion galaxies as a probe of AGN radiation in time and angle

William C. Keel^{1,2,3*}, Vardha N. Bennert⁴, Anna Pancoast^{5,6,7},
 Chelsea E. Harris^{5,8}, Anna Nierenberg^{5,9,10}, S. Drew Chojnowski¹¹,
 Chris J. Lintott^{12,13}, Kevin Schawinski¹⁴, Graham Mitchell¹⁵,
 and Claude Cornen¹⁵

¹*Department of Physics and Astronomy, University of Alabama, Box 870324, Tuscaloosa, AL 35487, USA*

²*Visiting Astronomer, Kitt Peak National Observatory, operated by AURA, Inc., under contract to the US National Science Foundation.*

³*SARA Observatory*

⁴*Department of Physics, California Polytechnic State University, San Luis Obispo, CA 93407, USA*

⁵*Department of Physics, University of California, Santa Barbara, CA 93106 USA*

⁶*Harvard-Smithsonian Center for Astrophysics, 60 Garden St., Cambridge, MA 02138 USA*

⁷*Einstein Fellow*

⁸*Department of Energy Computational Science Graduate Fellow, Department of Astronomy, University of California, Berkeley, CA 94720*

⁹*Center for Cosmology and AstroParticle Physics, 191 West Woodruff Avenue, The Ohio State University, Columbus, OH 43204, USA*

¹⁰*CCAPP Fellow*

¹¹*Department of Astronomy, New Mexico State University, Las Cruces, NM 11001, USA*

¹²*Astrophysics, Oxford University*

¹³*Adler Planetarium, 1300 S. Lakeshore Drive, Chicago, IL 60605*

¹⁴*Department of Physics, ETH Zürich, Switzerland*

¹⁵*Galaxy Zoo*

ABSTRACT

We present observations of active galactic nuclei (AGN) with close companion galaxies, in search of regions of the companions whose gas is photoionized by the AGN (which we term cross-ionization). This phenomenon can trace patterns of escape of ionizing radiation from AGN, and their time histories. From an initial set of 212 candidates, identified with the help of Galaxy Zoo participants, we obtained long-slit optical spectra of 32 pairs most likely to show cross-ionization. Among these, 10 systems show evidence of such cross-ionization based on emission-line ratios, in broad agreement with expectations if most AGN have ionization cones with 60deg opening angles. The distributions of companion galaxies with and without signs of cross-ionization are similar in estimated incident AGN flux, suggesting that such additional factors as geometry of escaping radiation and long-term variability control this facet of the AGN environment. This parallels conclusions for luminous QSOs based on the proximity effect among Lyman α absorbers. In some galaxies, mismatch between spectroscopic classifications in the common BPT diagram and ratios of weaker emission lines highlights the limits of common classifications in low-metallicity environments. We highlight properties of several systems with particularly strong evidence for cross-ionization – Was 49, NGC 5278/9, and UGC 6081 – and find a potentially fading AGN in the NGC 5278/9 system. Finally, we provide guidelines for further examination of these systems.

Key words: galaxies: Seyfert — galaxies: ISM — galaxies: active

1 INTRODUCTION

Important aspects of active galactic nuclei (AGN) are studied through the properties of surrounding gas on scales up to kiloparsecs, providing information otherwise inaccessible

* E-mail: wkeel@ua.edu

due to the small size of the central regions or the timescales involved. This is especially true of AGN with extended emission-line regions (EELRs), which span kiloparsecs in radial distance and often occur over broad angular ranges about the central source (Stockton et al. 2006). The frequent occurrence of (double) ionized clouds with triangular shapes was a key piece of evidence for some form of geometric unification involving Seyfert galaxies of types 1 and 2 (Antonucci 1993). Recently, the discovery of the 45-kpc cloud known as Hanny’s Voorwerp (Lintott et al. 2009, Schawinski et al 2010, Keel et al. 2012b, Schawinski et al 2015, Sartori et al. 2016) highlighted what had earlier been an abstract possibility: using EELRs to trace the history of radiation from AGN across the light-travel times to distant gas clouds. In this instance the gas has such high ionization levels that it must be illuminated by a luminous quasar 2 orders of magnitude brighter than the observed galaxy nucleus; a former quasar has faded dramatically within 10^5 years. A tailored search by Galaxy Zoo participants led to confirmation of 19 less luminous examples (Keel et al. 2012a, and later studies have identified analogous candidates for fading AGN detected via such ionization echoes at both lower and higher luminosity (Schirmer et al. 2013, Schweizer et al. 2013).

All these interpretations of EELR observations for properties of the AGN themselves are restricted by the distribution of the gas around the AGN host galaxy, with potential biases due to the relative orientations of the disc and AGN absorbing torus (whose axes are essentially uncorrelated; Schmitt et al. 2003) and obscuration due to dust in the galaxy disc. Indeed, Hanny’s Voorwerp and its fainter Galaxy Zoo analogs all have their EELRs as part of tidal debris (Keel et al. 2015). In this study, we use galaxy pairs containing AGN to explore the possibility of EELRs consisting of gas from a companion galaxy, which would not suffer the same biases in illumination, and would also not have the kind of radial density structure which might be found in gas associated with the AGN host itself, allowing more secure measurements of the angular pattern of escaping radiation and its time history than possible from gas within the AGN host itself. While the triggering of AGN by galaxy interactions remains contentious, many AGN are certainly located in interacting galaxy pairs, a fact which allows us to use companion galaxies as screens to view the emerging radiation from their active neighbors, which we will call cross-ionization.

The conditions for cross-ionization in galaxy pairs to be important were set out as early as Filippenko (1982), and have been briefly considered as interest in dual-AGN systems increased (Liu et al. 2011). In spectra with relatively large apertures, cross-ionization could mimic a relatively low-luminosity AGN (as was noted by Liu et al. 2011), while ionized gas from a companion could generate velocity asymmetries in survey spectra of the kind studied by Comerford & Greene (2014). One of the best candidates, Was 49ab, was observed in detail by Moran et al. (1992) who discussed the possibility of cross-ionization.

Similar issues - AGN episode lifetimes and the solid angle over which ionizing radiation escapes - have been addressed for QSOs by seeking changes in the ionization level implied by absorption lines from dense parts of the intergalactic medium (IGM), above all the H I and He II Lyman α forests (Furlanetto & Lidz 2011). A local source of hard

radiation, above the mean background at a QSO’s redshift, decreases the strength of these absorption features within a radius depending on the local AGN flux. This has been measured as the proximity effect - originally in the spectrum of the QSOs themselves, with redshift mapping to distance in front of the AGN, and later in the transverse proximity effect (Adelberger 2004, Kirkman & Tytler 2008, Gonçalves et al. 2008, Schirber et al. 2004) as the line of sight to the AGN observed passes close to a foreground AGN. Mismatch between these two kinds of proximity effect could result from episodic luminous AGN phases Visbal & Croft (2008) or anisotropic escape of the ionizing radiation.

Our approach complements studies of both proximity effects; close companion galaxies can probe to smaller separations and lower AGN luminosity than is feasible with the usually statistical nature of absorption-line studies. We rely on an analogous process: detection of ionization in excess of what sources other than the AGN can produce, in this case through changes in emission-line ratios as the AGN contribution becomes comparable to, or exceeds, that from star formation in a companion galaxy. The diffuse phase of the ISM is important here; at its typically low density, relatively few AGN photons can shift its ionization balance, in contrast to H II regions with higher densities of both particles and stellar ionizing photons. The contributions of these phases differ considerably among galaxies. For this reason, we use the expected ionizing flux from AGN at companion locations only as a relative guide to priority for observation.

We have conducted an extensive search for AGN cross-ionization candidates. This paper describes our sample selection, with participation from Galaxy Zoo volunteers, priorities among these based on physical properties, narrowband imaging of a subset, and spectroscopic observations, identifying a set of probable instances of cross-ionization between AGN and companion galaxies. In quoting luminosities and sizes, we adopt $H_0 = 70 \text{ km s}^{-1} \text{ Mpc}^{-1}$ and flat geometry.

2 SAMPLE SELECTION AND OBSERVATIONS

2.1 Sample criteria

For detectable cross-ionization of the ISM in a companion galaxy, both the impinging intensity of ionizing radiation from the AGN and the chances of the companion intercepting the pattern of merging radiation (i.e. ionization cones) are relevant. These are independent criteria, and we consider both in selecting the most promising targets. Our criteria are shown schematically in Fig. 1. Here, r is the projected separation from the AGN to the center of the companion, and θ is the angle the companion subtends in projection around the AGN. Galaxy size is not well-defined, particularly when images overlap so that standard photometric procedures may not separate galaxies properly; operationally we take the extent detected in composite images from the Sloan Digital Sky Survey (SDSS; Abazajian et al. 2009, Alam et al. 2015) for a consistent way to compare different systems. Spot checks show that this extends to a projected distance from the nucleus roughly equal to the SDSS quantity $petroR90_r$, and about 1.3 times the Petrosian radius $petroRad_r$.

Observed ionization cones have projected full opening

angles typically 70° (Wilson 1996, Keel et al. 2012a), half-angle $\approx 35^\circ$. Ignoring projection effects which are poorly-known for most objects, this implies that ionizing radiation emerges over a fraction ($1 - \cos 35^\circ = 0.18$) of the sky around atypical AGN, and suggests that we could expect roughly this fraction of companions to show cross-ionization if they are close enough for the incident AGN radiation to be suitable intense. This is a very crude estimate, since there is such a wide range of observed opening angles and projection factors will enter, but guides our expectations.

Also relevant to our selected number of cross-ionization cases is that fact that both r and θ are subject to projection effects due to the (essentially unknown) line-of-sight separation between the galaxy centers. We can estimate the typical magnitude of this effect in distance between galaxies in a pair, using a combination of the correlation-function slope ζ (which is consistent across the separations of galaxy pairs and groups), and a cut in projected radius (whose value is arbitrary since the correlation function is a power law). Using 10^4 Monte Carlo trials for pairs of points separating according to $\zeta \propto r^{-1.6}$, the mean projection effect is very poorly defined because of the long tail of widely-separated galaxies, but the median projection factor between projected and physical radii is stable at 1.52 (decreasing the inferred intensity of incident AGN radiation by a factor 2.3).

Ideally, we would seek companion galaxies with the rare combination of being rich in neutral gas to trace ionizing radiation, and poor in ongoing star formation which dilutes the emission lines of AGN-ionized gas. A selection on companion optical colours could eliminate “red and dead” systems on the red sequence which are very gas-poor, but this could also in principle eliminate some galaxies with enough gas for observable line emission (including H I clouds on the periphery of quiescent galaxies).

When both galaxy redshifts are known, we can filter many line-of-sight projections from candidates for genuine companion galaxies.

Since many galaxy pairs close enough for cross-ionization to occur are strongly interacting, gas in tidal tails or other debris can increase the cross-section of this process. As noted already, some known EELRs consist mostly of gas in such tidal features (Keel et al. 2012a, Keel et al. 2015). Even tidal tails arising in the disc of an AGN host galaxy can be twisted away from its plane far enough to escape obscuration by material in the inner disc of the host. In selection for spectroscopy, we consider tidal tails to be evidence of physical association even when the companion redshift was unknown.

2.2 Sample construction

We compiled a parent sample of AGN with companion galaxies based on the redshift and geometric criteria just discussed, largely through the efforts of volunteer participants in the Galaxy Zoo project (Lintott et al. 2008). A post on the project forum setting out the desired kinds of galaxy pairs led to responses beginning both from objects seen in the normal course of classification for Galaxy Zoo, and from SQL queries of the SDSS photometric and spectro-

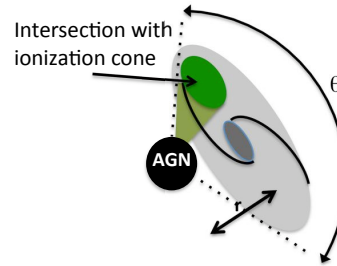


Figure 1. Schematic diagram of an AGN illuminating a large companion galaxy, showing the selection parameters r and θ . The projected separation r , combined with the AGN luminosity, predicts the strength of ionization expected at the companion, while its angular extent θ with respect to the AGN predicts the probability of ionization cones actually intersecting the companion galaxy. Both r and θ are subject to projection effects.

scopic catalogs¹. These suggested pairs were used as a starting point, further refined by inspection of spectra to confirm the presence of a clear spectroscopic AGN. We required a Seyfert nucleus; if a LINER AGN is present, its inferred ionizing luminosity would be lower than in Seyferts, making cross-ionization less effective. When only the AGN redshift is known, tidal distortion was taken as secondary evidence that two galaxies are physically associated. These factors led us to a finding list of 212 AGN/companion pairs (Appendix A), incorporating Galaxy Zoo forum postings between 16 January 2012 and 15 March 2014.

We also included a few nearby systems passing these tests, previously known outside the SDSS imaging region (i.e. Keel 1996 building on the catalog by Lipovetsky et al. 1988): NGC 2992, NGC 6786, Kaz 63, Kaz199

From this parent sample of 212 AGN/companion pairs, we used several criteria to rank them in observational priority. As defined in Fig. 1, we can measure θ and r , and estimate the ionizing luminosity based on the nuclear [O III] flux. We use [O III] rather than H α or H β , since the broad-line components can suffer obscuration in at least some Sy 2 nuclei; the [O III] luminosity is a nearly isotropic luminosity indicator based on its relation to mid- and far-IR selection (e.g. Keel et al. 1994). The [O III] fluxes are taken mainly from the SDSS spectra, augmented in a few cases by published data from other sources. We use these values only in a relative sense here, for ranking priorities; a conversion to absolute values is needed to predict individual values. When needed, we used the conversion between [O III] and bolometric luminosity from Heckman et al. (2004), an energy ratio 3500 between bolometric and observed [O III] output, and the mean radio-quiet spectral energy distribution (SED) from the QED project (Elvis et al. 1994), where the ionizing luminosity is about 0.14 of the bolometric value. These give predictions of the incident ionizing flux F_{ion} on companion galaxies from the AGN [O III] flux and companion geometry, which can suggest likely ionization parameters for

¹ <http://www.galaxyzooforum.org/index.php?topic=279841.0>

a particular ISM density. This estimate applies to the projected location of the companion nucleus; in some systems the range between near and far sides of a companion disc is very large.

For each spectroscopic observing session, we selected accessible pairs with either the highest predicted ionizing flux at the companion, or the largest projected angle θ spanned by the companion (translated to expected solid angle spanned by the companion as seen from the AGN).

When the companion spectrum is available (from SDSS or other sources as listed by NED), we omitted those with strong line emission from star formation, since weaker contributions from AGN-ionized gas become progressively more difficult to distinguish in composite systems. Previous dual-AGN candidates were retained in our list, since some of these may be instances of cross-ionization where the nucleus and surrounding ISM are blended in the SDSS spectrum (Liu et al. 2011).

Mkn 177 and its compact companion fit our selection criteria, but there is known to be no resolved line emission around the putative AGN, whose long-term variability suggests that it may instead be a very luminous, unusual variable star, or more speculatively, an ejected supermassive black hole leaving the site of interaction (Koss et al. 2014).

2.3 Observations: long-slit spectra

Cross-ionization should give spectroscopic signatures such as extended ionized gas with AGN-like line ratios across the companion, and ionization behavior not symmetric about the companion nucleus. We have carried out a spectroscopic study of candidate AGN in galaxy pairs to isolate a subset with these features.

We obtained spectra of 32 candidate pairs, some multiple times for confirmation or at different position angles, using the Kast double spectrograph (Miller & Stone 1992) at the 3-m Shane telescope of Lick Observatory during 13 nights from 2013–2015; the 2015 observations added exposure time or spatial coverage for cross-ionization candidates found in earlier sessions. For each session, the D46 dichroic beamsplitter separated light into blue and red optical paths, with a nominal split centered at 4600 Å. The wavelength settings were roughly 3400–4600 Å in the blue, and 4600–7400 Å on the red side. The slit width was 2.0 arcseconds. Flux calibration used observations of 1–3 standard stars per night.; clouds prohibited observing standards on 23 April 2015, so we used the response curve derived for 26 April, and scaled line fluxes in the case of SDSS 1354+1327 to match earlier data where the slits crossed at the nucleus. Systems observed on each night are listed in Table 1, and descriptions of the spectral characteristics of spatially resolved, extended line emission are in Table 2. The initial slit orientation crossed both galaxy nuclei, unless SDSS images suggested strong off-nuclear line emission via unusual *gri* colours, with further slit orientations in some cases when suggested by system structure or results of a first observation. Of the 32 systems we observed, 10 show evidence of extended AGN-ionized gas in companion galaxies or tidal tails.

To assess the dominant ionizing mechanism for detected regions, we rely on the approach pioneered by Baldwin et al. (1981), widely known as BPT diagrams. In particular,

star-forming objects and AGN are generally well separated in a diagram comparing the ratios of strong emission lines [O III] $\lambda 5007/\text{H}\beta$ and [N II] $\lambda 6583/\text{H}\alpha$. Specifically, we use the updated boundaries specified by Kewley et al. (2006). This single diagram, while relying on the spectral lines most easily detected in the optical, can become ambiguous at low metal abundances (as in some of the EELRs examined by Keel et al. 2012a). He II or [Ne V], when seen over large areas, are virtually certain indicators of photoionization by AGN radiation, but our data are only rarely sensitive enough to reveal these in the outskirts of the galaxies. Further, the wavelength range around He II $\lambda 4686$ at redshifts $z = 0.02 – 0.04$ (typical of the bright objects in this sample) is compromised by a night-sky emission line in spectra from Lick Observatory.

The long-slit results for objects with possible AGN ionization in the companion galaxies (or tidal tails) are presented in Fig. 2. Spectral properties were evaluated using Gaussian fits to 2-pixel (1.5") sums along the slit. The top panels show the slit locations in these systems superimposed on composite SDSS *gri* images. The middle panel for each spectrum shows the redshift behavior (heliocentric cz) along the slit as well as intensity slices in the continuum and [O III] (or $\text{H}\alpha$ for two cases where it was detected much more widely - NGC 3341 and UGC 6081). The bottom panels show the strong-line BPT diagram with the star-forming/AGN boundary from Kewley et al. (2006); the colours of points match between the velocity plots and BPT diagrams to show where the AGN-ionized regions occur along the slit. Because of the larger flux and smaller correction for underlying stellar absorption, we simply estimate the flux of $\text{H}\beta$ from that of (narrow-line components of) $\text{H}\alpha$ and a Balmer decrement of 2.85; with this approach, reddening correction will move data points further into the AGN region in these line-ratio diagrams.

The strong-line BPT diagrams, while allowing examination of the most extensive areas, may be misleading when low-metallicity gas is involved, such as is encountered in tidal debris and the outer discs of spirals. AGN photoionization models with varying abundance (with oxygen and nitrogen having the strongest signatures) show that nitrogen abundances below solar can move AGN-ionized gas into parts of the usual BPT diagrams occupied by star-forming regions (Storchi-Bergmann et al. 1998, Castro et al. 2017); in particular, [N II] and [S II] weaken at fixed [O III]/ $\text{H}\beta$. So, while AGN-ionized gas may be securely identified if its strong-line ratios place it in the “AGN” region of the BPT diagrams, lower-metallicity counterparts may require additional information for secure classification. Significant He II or [Ne V] emission can play such a role, but these lines are comparatively weak in AGN narrow-line regions, and would not be detected outside the nuclei in most of our spectra. The [O I] $\lambda 6300$ line is detected in some of our spectra and can help resolve this ambiguity.

2.4 Observations: narrowband imaging

Our spectroscopy is supplemented by narrowband imaging for 7 systems, summarized in Table 3. For seven of the objects with the highest priority for spectroscopic observations in the redshift range $z = 0.008 – 0.027$, where [O III] falls in the band of an averrable filter, we obtained images in red-

Table 1. Spectroscopic observations

UT Date	Galaxies observed
Jan 15 2013	0057+0120,0848+3515
Jan 16 2013	0029+0010,0848+3515, 1214+2931
Jan 17 2013	0029+0010 compn,0757+3511,0848+3515,1200+147
Jan 18 2013	0057+0120,0841+0101,0905+3237,1010+0612,1352+2528
Mar 10 2013	0838+0407,0847+3445,0904+5536,1138+1412,1201-0153,1303-0306,1354+1327
Mar 11 2013	0904+5536,1213+5138,1243+3738,1342+1839,1347+1734,1354+1327
Mar 12 2013	1050+2329,1219+1326, 1414-0000
Mar 13 2013	1042+0502,1101+1017,1132+5257,1142+3251, Kaz 199
Feb 4 2014	0839+4707, UGC 6081, NGC 5279
Feb 5 2014	0838+0407, UGC 6081,NGC 5279
23 April 2015	0848+3515, 1354+1327, NGC 3341, Was 49, NGC 5279
24 April 2015	NGC 3341, 1354+1327
26 April 2015	1201-0153, NGC 3341, NGC 5279, UGC 6081, Was 49

Table 2. Spectroscopic summary

AGN	Type	z	PA°	Description
Candidate cross-ionization systems				
SDSS J002944.89+001011.1	Sy 2	0.0598	49	Line emission extended across pair. Compn [O III]/H β drops to ≈ 2.5 (UM 246)
SDSS J005754.03+012013.8	Sy 2	0.0567	168	Extended high-ionization emission from AGN to companion seen in [O III], H α (UM 293)
SDSS J083902.96+470756.3	Sy 2	0.0524	56	Extended high-ionization emission
SDSS J084810.11+351534.3	Sy 2	0.0573	72, 107	2nd Sy 2 or cross-ionization, AGN line ratios across extended region (KUG 0845+354)
SDSS J104232.05+050241.9	Sy 2	0.0272	98, 212	Very ext emission into compn (H II ratios but has [O I]) = NGC 3341
SDSS J110019.10+100250.7	Sy 2	0.0361	133, 134	UGC 6081; AGN-ionized cloud
SDSS J120149.74-015327.5	Sy 1	0.097	139,142	AGN is Sy 1.9 w/ionized tail opposite compn. Compn looks like H II.
SDSS J121418.25+293146.7	Sy 2	0.0632	60, 147	Was 49; 2nd AGN or cross-ionization, He II in 2nd nuc, (more distant ion from weaker nuc)
SDSS J134143.75+554025.5	Sy 2	0.0251	98	NGC 5278/9; high [O III]/H β , source unclear
SDSS J135429.05+132757.2	Sy 2	0.0633	84, 186, 194	Both galaxies have similar line ratios; [O III] tail opposite compn. Compn em extends pa
Other systems:				
SDSS J075729.04+351105.9	Sy 2	0.1117	99	double spatial/spectral line profiles
SDSS J080004.05+232616.2	Sy 2	0.0292	118	velocity structure in small emission region around AGN
SDSS J083848.14+040734.0	Sy 2	0.0476	96	AGN emission extended 5" toward H II compn
SDSS J084135.08+010156.2	Sy 2	0.1106	48	two AGN, extended [O III] beyond each
SDSS J084742.44+344504.4	QSO	0.0640	20	H α rotn curve over 60 pixels, no [O III] = PG 0844+349
SDSS J090436.92+553602.9	Sy 1	0.0372	7	emission around AGN extended by 15", more toward companion. No em in compn proper
SDSS J101043.36+061201.4	Sy 1	0.0978	58	[O III] resolved over 8". Weak em in compn, no [O III]
SDSS J105030.47+232931.4	Sy 1.8	0.0604	117	AGN unresolved. H II compn w/velocity gradient. Distant matching-z compn
SDSS J110157.90+101739.3	Sy 1.5	0.0341	138	extended rotn curve over 29", H II ratios
SDSS J113240.25+525701.3	Sy 2	0.0266	75	AGN extended to 6" away from 2 compns (Mkn 176)
SDSS J113858.89+141253.2	Sy 2	0.085	10	compn has resolved line em w/H II ratios
SDSS J114252.83+325124.2	Sy 2	0.0666	165	Compn - extended rotn curve, H II ratios
SDSS J120041.39+314746.2	Sy 2	0.1159	33	AGN emission spans 14", blends w/compn
SDSS J121303.34+513854.9	Sy 2	0.0849	118	AGN unresolved. Compn H II ratios, resolved.
SDSS J121943.13+132659.9	Sy 2	0.0647	50	AGN em unresolved, compn has [N II] and Balmer absn. Higher-z galaxy on slit
SDSS J124322.55+373858.0	Sy 2	0.0859	120	LINER-like AGN em to 8" opposite H II compn.
SDSS J130354.71-030631.8	Sy 2	0.0778	166	AGN emission not well resolved.
SDSS J134203.48+183901.5	Sy 1.8	0.085	102	AGN em (low-ion NLR) opposite compn to 8". Compn H II ratios, velocity gradient
SDSS J134736.39+173404.6	Sy 2	0.0447	108	AGN-ion knot at 18" opposite compn? Compn H II ratios, velocity gradient
SDSS J135255.67+252859.6	Sy 1.5	0.0636	176	Strong lines like starbursts, but He II/H β ≈ 0.2 and broad H α
SDSS J141447.15-000013.1	Sy 2	0.0475	65	Sy 2 plus transition nuc w/[O III]/H α ≈ 20 . Em not resolved.
Kaz 199	—	0.0155	5, 54	[O I]/H α ≈ 0.03 , may not be AGN

shifted [O III] and the V-band continuum using the SARA 1-m remote telescope at Kitt Peak, Arizona and the 1-m Jacobus Kapteyn telescope at La Palma, now operated by SARA (Keel et al. 2017a). Narrowband exposures in a filter of 100-Å FWHM were 1-2 hours total, with 15-30 minutes

in V. Among these, we recover the well-known ionization cones in NGC 2992 (Wehrle & Morris 1988, Allen et al. 1999, Veilleux et al. 2001) perpendicular to its disc plane (but not oriented toward either its tidal tail or companion). We find only nuclear emission from Mkn 176. NGC 3786/8

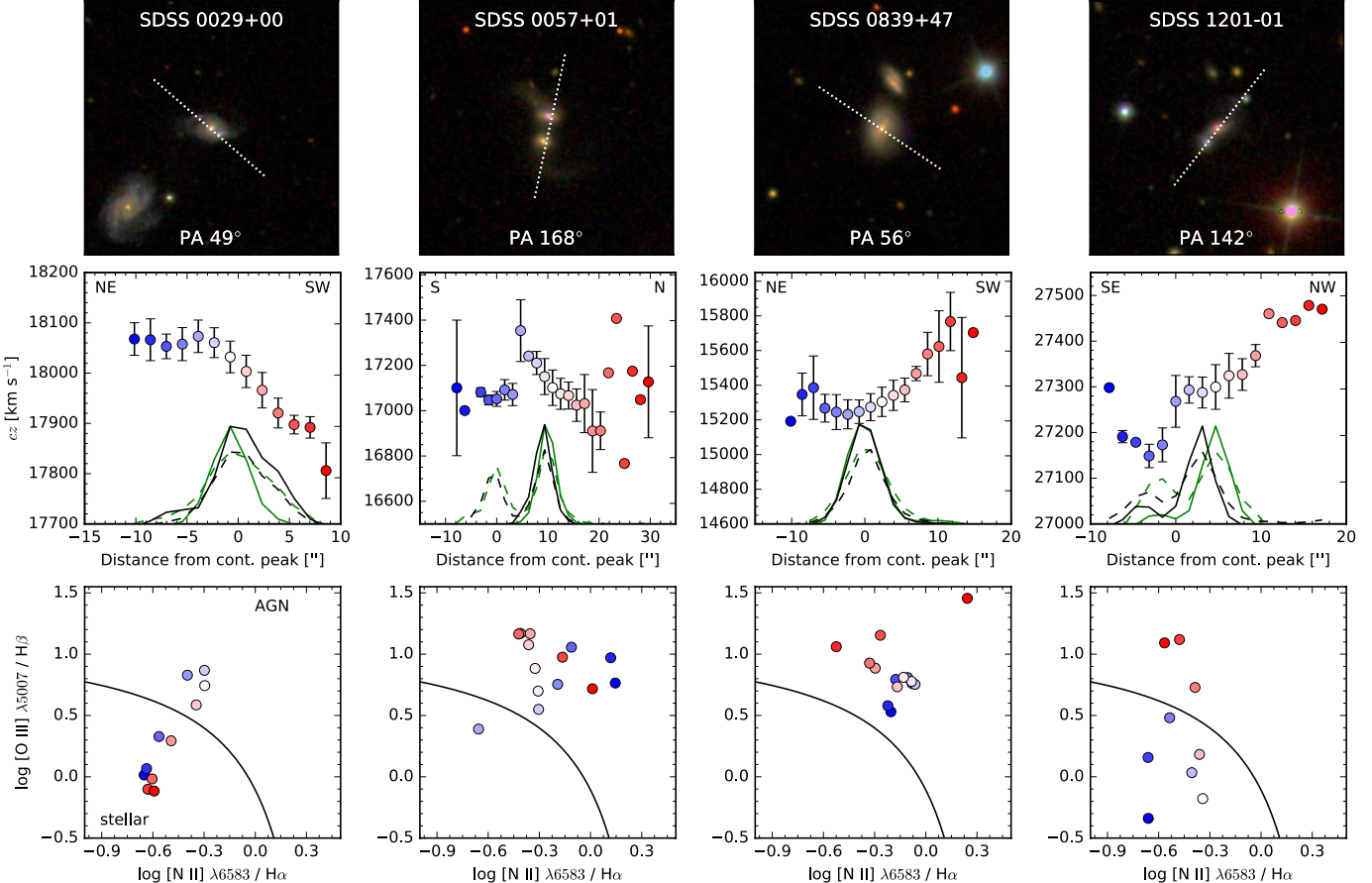


Figure 2. Results of long-slit spectroscopy of candidate AGN cross-ionization systems. For each object, the top panel shows the slit position on an SDSS DR12 *gri* composite image spanning $100 \times 100''$. The middle panel shows the heliocentric radial-velocity profile along the slit, with error bars based on agreement among multiple lines measured at each position, and colour coding of points to indicate position. Below the velocity profiles are intensity traces of [O III] (or H α for NGC 3341 and UGC 6081) and the continuum, on arbitrary linear vertical scales, to show the alignment between intensity and velocity features. The bottom panels show the strong-line BPT classification diagram with the starburst/AGN dividing curve from Kewley et al. (2006); point colors here show where along the slit AGN-ionized regions occur in comparison with the middle panels. The H β flux was estimated from H α and the intrinsic Balmer decrement 2.85; additional reddening correction would move data points upward and toward (or further into) the AGN-ionized region above the curves. Regions appear in this panel only if H α , [O III] and [N II] are all detected.

and UGC 3995 A/B show [O III] emission only from the nuclei and knots in the spiral arms, as is typical for spirals. On this basis, we did not obtain new long-slit spectroscopy of Mkn 176, NGC 2992, NGC 3788, or UGC 3995.

NGC 3341 shows a potential morphological signature of cross-ionization. The AGN here is in a small galaxy projected against the disc of a much larger spiral. In [O III], there is a triangular region of emission crossing the large disc at a skew angle with its apex at the AGN (Fig. 3), which we tentatively interpret as an ionization cone of gas in the large galaxy. The slit location for spectroscopy was selected to sample this region, rather than crossing the nucleus of the large companion galaxy.

Motivated by extended [O III] structure in our SARA images of Kaz 199, we obtained more detailed images with

the KPNO 2.1-m telescope. [O III] was isolated with a filter of 174 Å FWHM centered at 5142 Å, and H α with a filter of 68 Å FWHM centered at 6653. V and R were used for continuum subtraction.

For NGC 5278/9, we also analyze the H α and continuum images from the KPNO 2.1-m telescope described by Kennicutt et al. (1987), which guided our slit placement on noting that this pair was included in the AGN/companion sample. Our spectroscopic data, targeted to encompass one of these radial filaments, help interpret the nature of the emission filaments mentioned by Keel et al. (1989). Additional [O III] data were obtained with the SARA system.

For galaxies or regions with large enough equivalent width in the [O III] lines, we can produce [O III] images from linear combinations of the SDSS survey images (as shown by

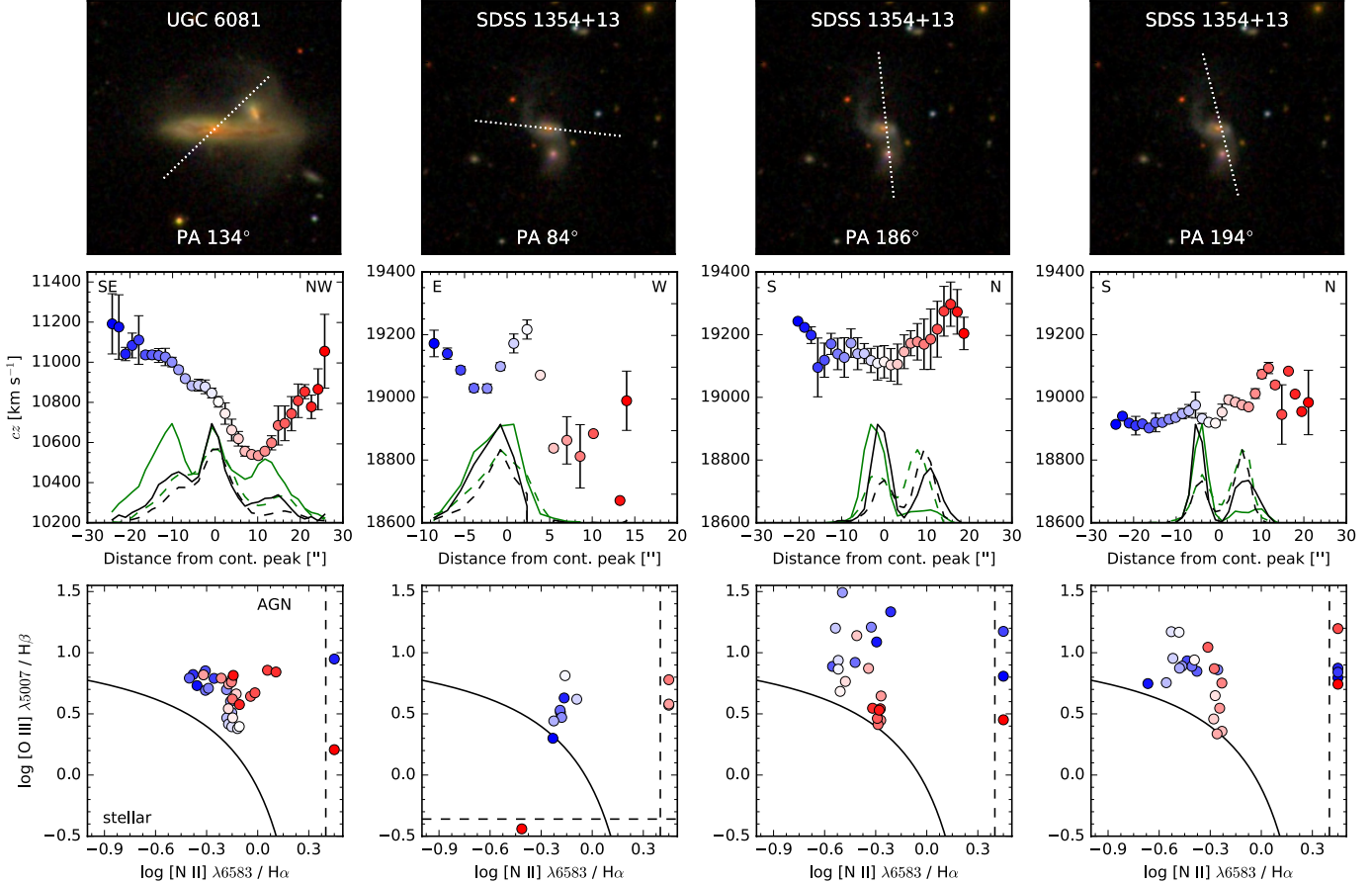


Figure 2 – continued

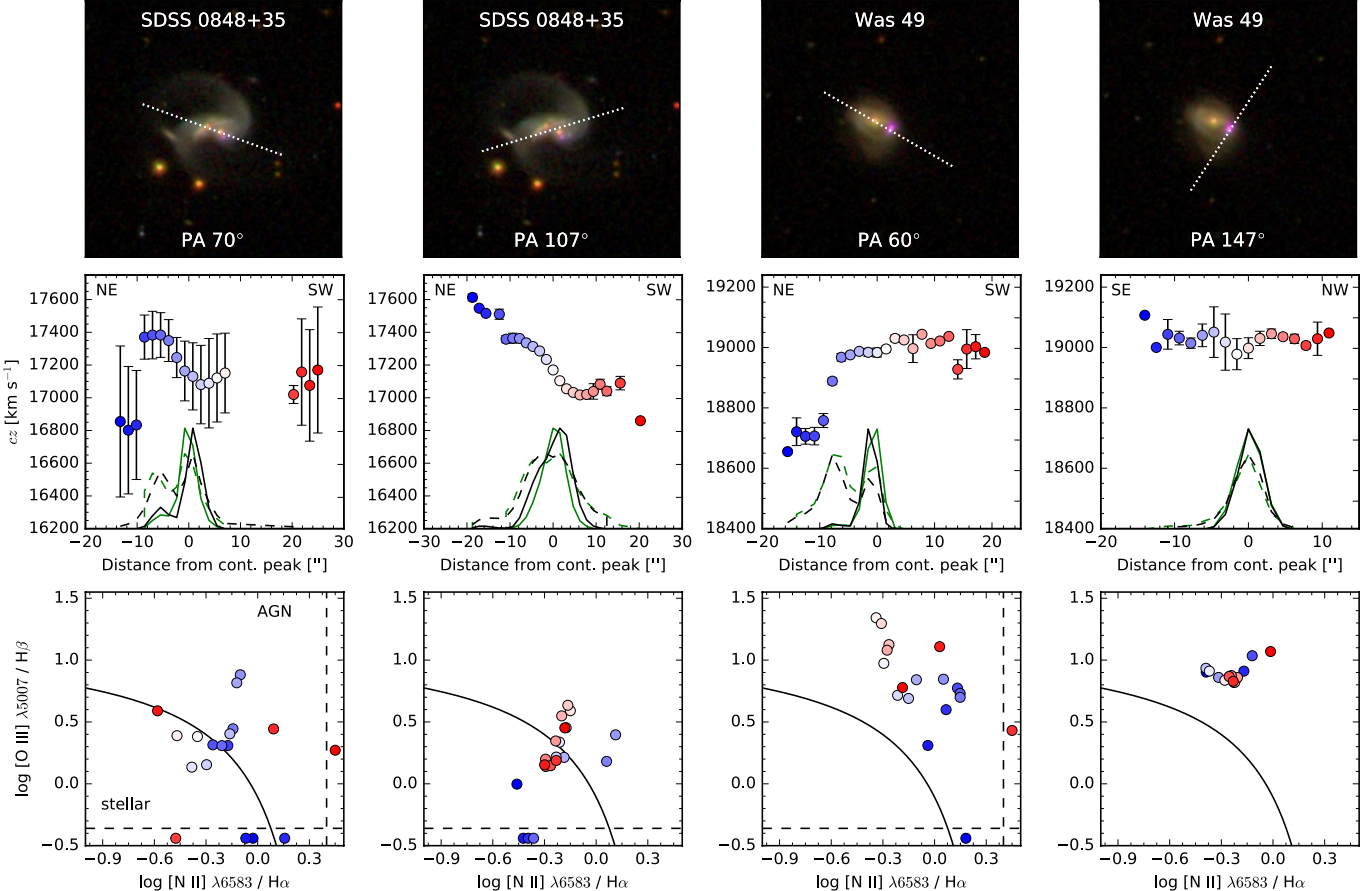
Table 3. Narrowband imaging

Object	z	Bands	Exposure [min]	Telescope	UT date
Kaz 199	0.0155	V/510	20/30	SARA-KP	25 Feb 2012
Kaz 199	0.0155	V/514	10/30	KPNO 2.1m	13 Apr 2013
Kaz 199	0.0155	R/6653	10/45	KPNO 2.1m	29 May 2012
Mkn 176	0.0274	V/510	20/60	SARA-KP	12 Mar 2013
NGC 2992	0.0077	V/510	15/120	SARA-KP	2 Feb 2013
NGC 3341	0.0273	V/510	30/120	SARA-KP	2 Feb 2013
NGC 3341	0.0273	V/510	20/60	SARA-KP	29 Dec 2014
NGC 3341	0.0273	B/V	30/30	SARA-JKT	4 Feb 2017
NGC 3786	0.0089	V/510	20/60	SARA-KP	4 Apr 13
NGC 5278/9	0.0251	6000/6693	10/20	KPNO 2.1m	18 May 1985
NGC 5278/9	0.0251	V/510	10/60	SARA-KP	27 Mar 2015
UGC 3995	0.0158	V/510	20/60	SARA-KP	31 Dec 2013

Keel et al. 2012a). We do this for Was 49 (Fig. 4), revealing extensions from the AGN in opposite directions, possibly including gas in the large companion disc.

3 CROSS-IONIZATION (AND MISSING-IONIZATION) CANDIDATE SYSTEMS

Several of the systems in Table 2 show evidence of cross-ionization. Others show no such evidence despite high *a priori*

**Figure 2 – continued**

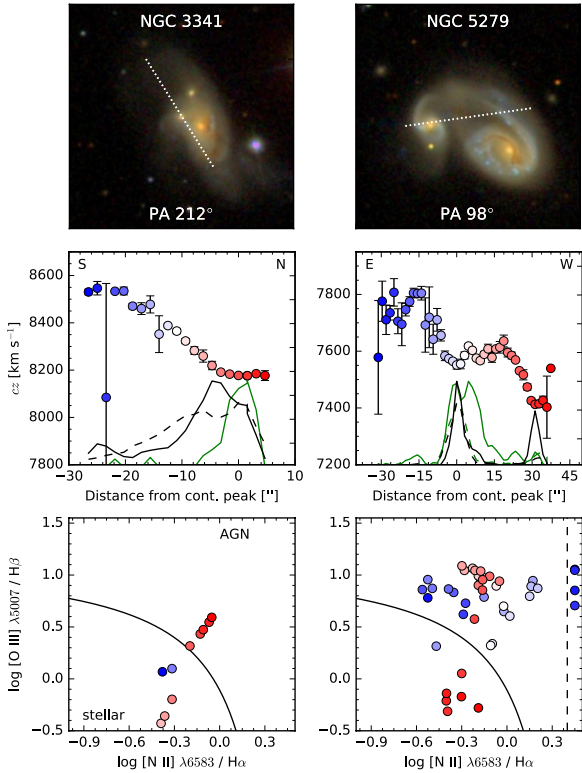
ori odds of seeing it from the system properties. We discuss some of their individual properties here.

Was 49: Identified in this context by Moran et al. (1992), this may remain the best low-redshift cross-ionization candidate. Detailed study of the AGN by Secrest et al. (2017) stresses its high luminosity and implied black-hole mass relative to the very modest stellar mass of the host galaxy. The [O III] structure around the AGN is elongated perpendicular to the line between the galaxies (Fig. 4); the images in Secrest et al. (2017) show that part of this emission is in a single bright discrete source just northwest of the AGN. All the locations along our spectroscopic slits in this pair are AGN-ionized except the nucleus of the large companion galaxy; the AGN emission is largely continuous with the portion of the large galaxy’s rotation curve sample in our data. Integral-field spectroscopy with high angular resolution could show whether the gas seen surrounding the AGN on arc second scales kinematically matches either its own radial velocity or the rotation pattern of the larger disc. In the latter case, the ionization pattern in the disc might reflect the pattern of escaping ionizing radiation.

NGC 5278/9: This pair has two low-luminosity AGN,

near the Sy 2/LINER boundary in line-ratio diagrams depending on aperture size. The system shows extensive filaments or plumes in line emission, some almost radial (Keel et al. 1989, Fig. 5). Our spectroscopy shows AGN-ionized gas across the pair, including one of these plumes to the east. This may suggest that either the AGN are heavily obscured along our line of sight or have faded. Because gas in each disc may be largely shielded from its own AGN, this pair is a potential instance of cross-ionization.

In this system, we have the data to estimate both the nuclear luminosities and the ionizing-flux requirement at various points in the extended emission, to see whether the nuclear output has changed dramatically over the relevant light-travel time, and how important obstruction of the AGN is long our line of sight. Since these nuclei were not observed spectroscopically in the SDSS, we use the optical emission-line data within 4.7 arcseconds reported by Keel et al. (1985). For mid-infrared nuclear properties, we take the PSF-fitting WISE fluxes (Wright et al. 2010), using the “compromise” spectral slope conversions from Cutri et al. (2012) and bearing in mind the potential non-nuclear contribution within the WISE PSF. Conversion from H α surface

Figure 2 – *continued*

brightness in extended regions to required luminosity in the ionizing continuum followed Keel et al. (2012a). To be conservative, we take the distance from extended cloud regions to each nucleus to be in the plane of the sky, minimizing the ionizing-luminosity requirements. The quantities involved in this comparison are given in Table 4.

This kind of estimate gives only a lower bound to the required ionizing luminosity of the AGN at the relevant time, both because a given parcel of gas is unlikely to be optically thick at the Lyman edge, and because we measure spatially averaged surface brightness in structures that are likely to be very patchy. For example, Gagne et al. (2014) and Keel et al. (2017b), working at a linear resolution of ≈ 150 pc from HST imaging of the ‘‘Teacup’’ AGN, find that this calculation for the brightest regions underestimates the ionizing continuum by about a factor 3 over a wide range in radius. For NGC 5278/9, we average over a yet larger region, roughly 2 kpc in size. Lacking more detailed information on the fine structure in NGC 5278/9, we consider that the multiplication factor will be at least 3.

SDSS 0057+01: AGN-ionized line ratios extend over most of the region sampled in both galaxies. The outermost parts at both ends of the slit are kinematically distinct from the rotational signature of the AGN host itself.

SDSS 0839+47: our spectrum across the AGN host shows that the AGN ionizes gas across the galaxy, with increasing ionization in the outer parts. The SDSS spectrum of the companion galaxy shows line ratios indicating star formation, albeit with [O I] rather strong at about $0.07 \times \text{H}\alpha$, broadly consistent with mixed ionization sources. This system was flagged by Comerford & Greene (2014) for showing

velocity asymmetries in both Balmer and forbidden emission lines.

SDSS 0848+35: there is an isolated region of AGN-ionized gas at a projected radius 21'' (23 kpc).

SDSS 1354+13: both galaxies show similar line ratios, marking a possible dual AGN system flagged by Liu et al. (2011) from the SDSS spectrum, and with a velocity asymmetry in the SDSS spectrum noted by Comerford & Greene (2014). AGN-ionized gas is more extended than the starlight continuum, notably in the tidal tail to the south, where it is detected to a radius of 22'' (27 kpc) along two adjacent slit positions. Comerford et al. (2017) recently presented a suite of spectroscopic data showing both an EELR and a spatially resolved outflow, with implied timescales suggesting recurrent episodes of nuclear activity. Their EELR detection south of the nucleus overlaps with our data along the N–S slit position; our data extend slightly farther from the AGN.

NGC 3341: This pair has nearly the ideal geometry from Fig. 1, with an AGN hosted in a compact galaxy close to a much larger spiral (Barth et al. 2008). In a multiwavelength study, Bianchi et al. (2013) set very low limits on AGN in the other components of this system. Our emission-line imaging (Fig. 3) shows a possible ionization cone in [O III] southward from the AGN across the larger disc. However, the spectroscopic data show AGN ionization dominant only close to the AGN, so this structure may be an accident of the spiral pattern and location of star-forming regions. On the other hand, the spectrum shows [O I] on the strong side for pure stellar photoionization across much of this region, with $[\text{O I}] \lambda 6300/\text{H}\alpha \approx 0.03$. More detailed data and modeling would

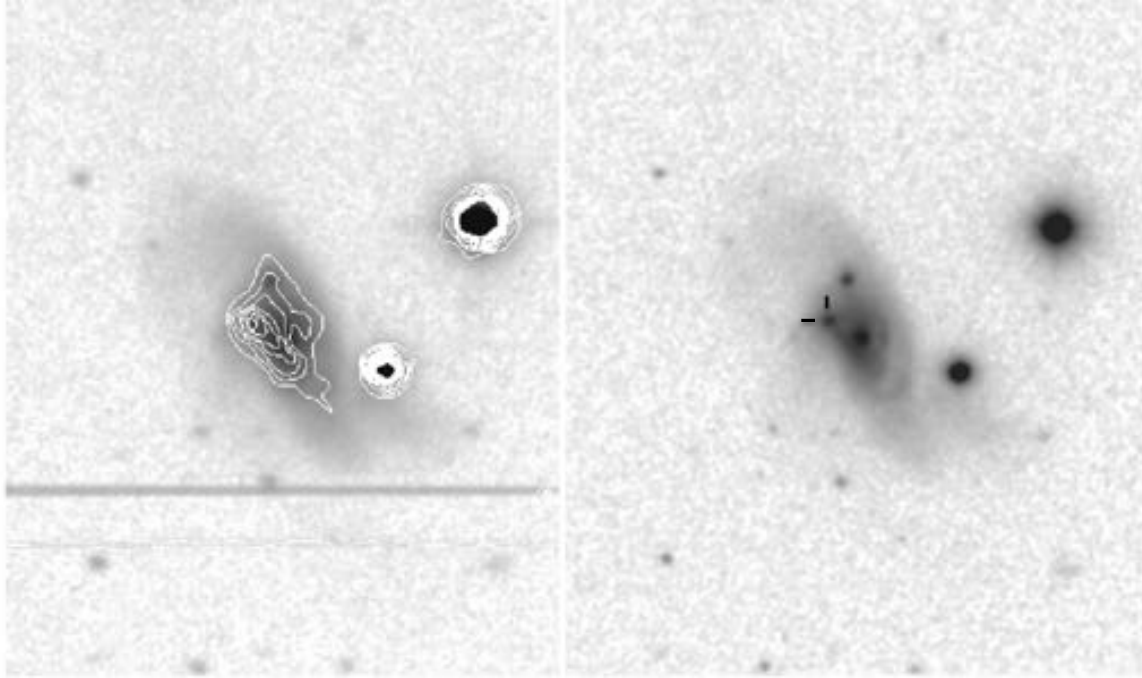


Figure 3. [O III] structure (linearly spaced contours) superimposed on the matched-resolution V -band continuum of NGC 3341, with a higher-resolution V image from the JKT also shown for comparison of the inner structure. The Seyfert nucleus in this system is in the small companion galaxy to the east (indicated by tick marks in the right-hand panel); the [O III] structure may represent an ionization cone comprised of material mainly in the disc of the large galaxy. Stellar residuals result from colour differences between foreground stars and the galaxies; two bright-star charge trails are seen on the southern side. The area shown is $167 \times 201''$, with north at the top. The intensity mapping in V uses a logarithmic scale offset from zero to avoid amplifying noise around the sky level.

Table 4. Recombination-balance analysis

Quantity	NGC 5278	NGC 5279	UGC 6081 SE	UGC 6081 NW
$H\alpha$ flux, nucleus ($\text{erg cm}^{-2} \text{s}^{-1}$)	2.17×10^{-15}	2.20×10^{-15}	5.09×10^{-14}	2.86×10^{-13}
[O III] $\lambda 5007$ flux, nucleus ($\text{erg cm}^{-2} \text{s}^{-1}$)	9.7×10^{-15}	1.2×10^{-14}	1.6×10^{-14}	1.44×10^{-13}
$L(\text{ion})$ from [O III] (erg s^{-1})	4.9×10^{42}	6.2×10^{42}	9.4×10^{43}	1.9×10^{44}
$Q(\text{ion})$ from [O III] (photons s^{-1})	1.1×10^{53}	1.4×10^{53}	2.2×10^{54}	4.4×10^{54}
$F(\text{MIR})$ (8-25 μm) ($\text{erg cm}^{-2} \text{s}^{-1}$)	1.5×10^{-11}	8.5×10^{-12}	2.2×10^{-11}	3.0×10^{-11}
$L(\text{MIR})$ (erg s^{-1})	1.5×10^{43}	8.8×10^{42}	6.3×10^{43}	8.6×10^{43}
Max $L(\text{ion})$ (erg s^{-1})	2.0×10^{43}	1.5×10^{43}	1.6×10^{44}	2.8×10^{44}
Extended region needs:				
$L(\text{ion})$ (erg s^{-1})	$> 4.2 \times 10^{43}$	$> 1.4 \times 10^{43}$	$> 9.4 \times 10^{43}$	$> 1.9 \times 10^{44}$
$3 \times$ structure correction (erg s^{-1})	1.3×10^{45}	4.2×10^{44}	2.8×10^{44}	5.7×10^{44}

be needed to tell whether this is low-metallicity gas ionized by an AGN, a composite of both ionization sources blended along the slit, or something yet more complex.

UGC 6081: This pair has two heavily reddened Sy 2 nuclei and shows AGN ionization along an extent of 58" (41 kpc). The extended emission might fall in the same

category of radial extent > 10 kpc as the “Voorwerpjes” (Keel et al. 2012a), depending on which of the AGN lights it up. We do not have the three-dimensional information to tell which is responsible (if indeed one dominates in the tidal debris seen at large radii). We do have the information for a rough ionization-balance calculation as done above for

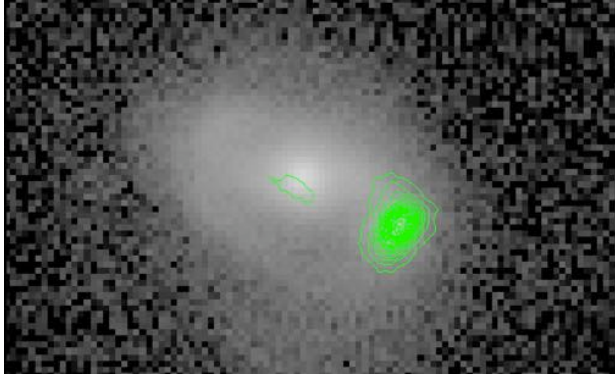


Figure 4. [O III] structure (contours) superimposed on the the *r*-band image of Was 49, from SDSS data using the difference between *g* and *r* data to trace line emission. The Seyfert nucleus in this system is in the small companion galaxy to the west, superimposed on the large companion disc and centered in the contours; the [O III] structure may represent an ionization cone. The area shown is $26 \times 45''$, with north at the top.

NGC 5278/9. These nuclei are more luminous and much more heavily reddened than in NGC 5278/9; straightforward screen reddening and the nuclear Balmer decrements suggest that the NW AGN, in the smaller galaxy (UGC 6081 NED01), is twice as luminous in [O III]. Our estimates (Table 4, listing dereddened values in this system) show that the energy balance makes it plausible for the SE AGN (in UGC 6081 NED02) to power the most distant gas we observe spectroscopically along the slit to its southeast, although whether this works in detail depends critically on the fine structure of the gas (since the peak surface brightness we observe places the strongest limits on the incident flux, and is strongly dependent on image quality). Much of the reddening toward each nucleus may take place close to our line of sight rather than as surrounding ‘‘cocoons’’ covering large solid angles; the WISE data suggest that in neither one does the MIR component of the SED dominate over ionizing radiation reaching surrounding gas. Using our conservative fine-structure correction (a factor 3 as noted above), the case for AGN fading in this system is weak (energy shortfall 1.7–2.0 times depending on which AGN is responsible, and no shortfall if both contribute to the ionization of the extended cloud).

NGC 6636 = Kaz 199: the small northeastern component of this pair (outside the SDSS footprint) has been catalogued as a Seyfert galaxy. We are unaware of a previously published spectrum of the AGN. In our new data, the strong lines would classify both galaxies as star-forming, but [O I] has intensity $\approx 0.05 \times \text{H}\alpha$ across a large region, at the very high end of values seen in disc H II regions and potentially a sign of composite ionization sources. In our [O III] images, the small galaxy (with reported AGN) is surrounded by an arc of emission-line knots (Fig. 6), in addition to the region tracing the tidally distorted arms of the larger galaxy. The sizes of these knots are consistent with unresolved H II regions, rather than the filamentary appearance often seen

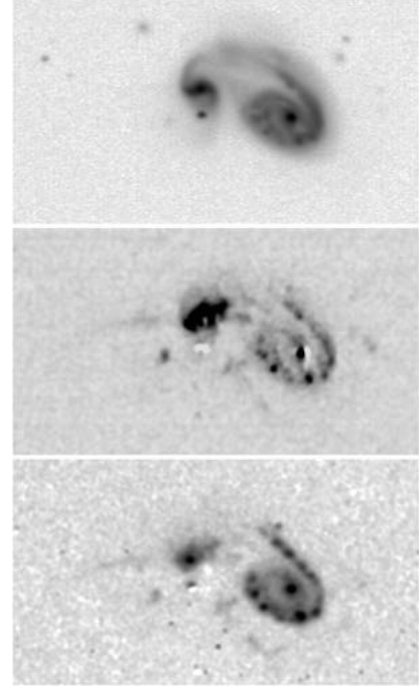


Figure 5. The NGC 5278/9 system in the *V* band (top), continuum-subtracted [O III] (middle), and continuum-subtracted H α +[N II] (bottom). The field shown is $141''$ across with north at the top. PSF mismatches give artifacts at the locations of bright stars and the galaxy nuclei. At least three partly radial emission features are present without significant continuum counterparts; our spectrograph slit crossed the nucleus of NGC 5279 (left) and included much of the emission feature extending to its east. The intensity scales are logarithmic starting at levels slightly offset from zero.

in giant AGN-ionized clouds (Keel et al. 2012a, Keel et al. 2015).

Some systems attract attention because of what we don’t see. The best example is SDSS J084742.44+344504.4, also catalogued as PG 0844+349, a QSO with a nearby large spiral companion galaxy projected $25''$ away (32 kpc). Fig. 7 shows the velocity structure of this companion galaxy to the southwest, along its projected major axis. [O III] is detected only at the two positions in its disc where the slit crosses the spiral arms, weaker than H α , so there is no evidence of external AGN ionization. An HST archival image (from Barth et al., program 9763) shows this to be a very symmetric, inclined grand-design spiral, similar in scale to the QSO host galaxy itself (Fig. 8). The outer arms are so open in comparison to the inner structure that they may be tidally induced; the dust lanes on the northern side of the arms plus the velocity slice show that the spiral pattern is trailing. The slit spectroscopy by Hutchings & Crampton (1990) shows only weak emission in the southern spiral arm of the QSO host, without an obvious enhancement as the slit crosses the west-

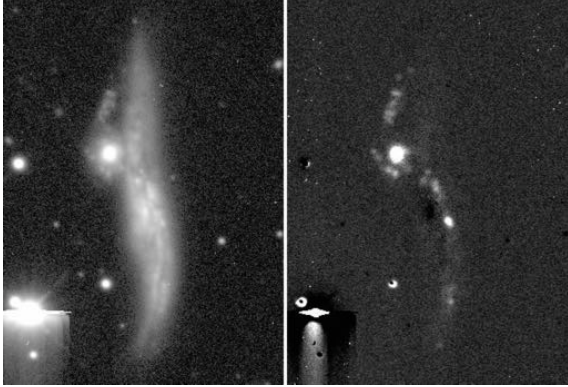


Figure 6. V -band continuum (left) and subtracted [O III] (right) images of Kaz 199 = NGC 6636 from the KPNO 2.1m telescope. A saturated star produced artifacts at lower left, and the colour changes associated with the dust lane in front of the bulge give negative residuals near the nucleus of the larger galaxy. The reported AGN is in the small companion galaxy to the northeast (upper left).

ern arc, so this feature more likely consists of star-forming knots rather than AGN photoionization which fits as well with its very knotty structure compared to the more diffuse and filamentary appearance of EELRs, as in Keel et al. 2017b). These data, and our results on the spiral companion, fit with ionization cones directed near the line of sight and out of the plane of the host galaxy or intermittent high-luminosity accretion phases, perhaps combined with a large physical separation between the pair members. While there remains substantial uncertainty in the line-of-sight separation, this galaxy pair may furnish an emission-line version of the same issues encountered in comparing IGM ionization via the direct and transverse proximity effects (as summarized in the Introduction).

Its F_{ion} and projected separation would be very favorably for cross-ionization, but we see no evidence of this. The companion could be at a larger line-of-sight separation (up to the level indicated by the small Δz), lie entirely outside an ionization cone, or fall outside radial zones which we could see ionized by an episodically luminous AGN.

Our primary tool for recognizing AGN-ionized gas is the set of strong emission-line ratios in the “classical” BPT diagram (Baldwin et al. 1981), based on [O III]/H β and [N II]/H α , incorporating the revised class boundaries from Kewley et al. (2006). These diagnostics become less certain at lower metallicity as [N II] and [S II] become weaker. In this sample, for example, the BPT diagram would classify both SDSS J134203.48+183901.5 and SDSS J135255.67+252859.6 as star-forming galaxies, but broad H α in the first case, and strong and narrow He II $\lambda 4686$ in both, mark them as AGN.

Among objects selected for spectroscopy, the ranges and median values of F_{ion} are similar for the subsets with and without evidence for cross-ionization; for example, the Kolmogorov-Smirnov test suggests rejection of the hypothesis that the distributions are identical only at significance

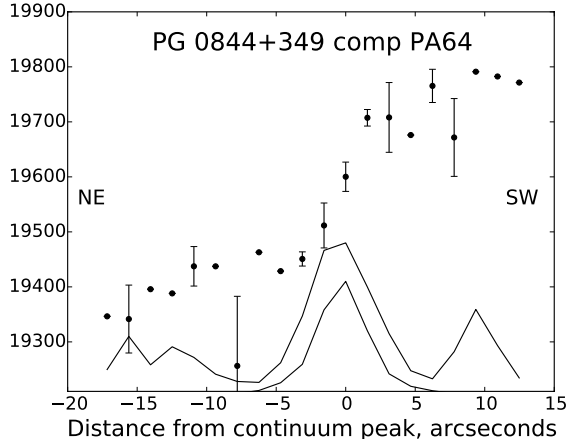


Figure 7. Spectroscopic results on the southern companion to PG 0844+349, shown as in Fig. 2. The traces across the bottom show the continuum and (more extended) H α intensities.

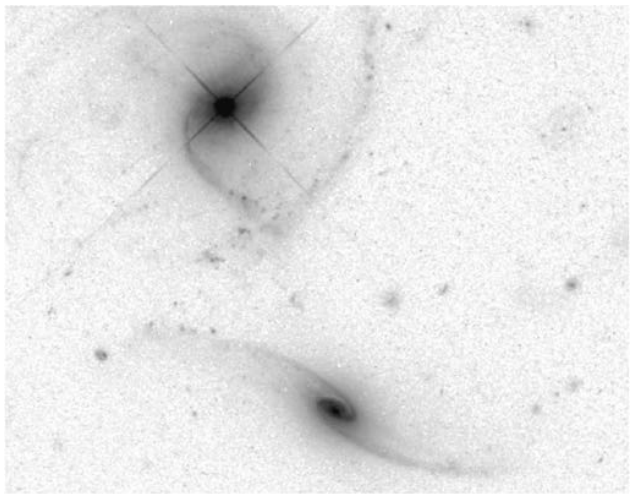


Figure 8. Archival HST image of PG 0844+349 and companion galaxy to its south, from Barth et al. program 9763. This is part of an ACS WFC image in the F625W filter, smoothed with a 3-pixel median for cosmetic reasons. The redshifts are a close match, with the companion at $z = 0.0652$ compared to the luminous AGN at $z = 0.0643$ for a projected velocity difference near 270 km s^{-1} . As expected for trailing spiral arms and the visible dust on the north side, the NE side of the disc is approaching. The area shown spans 38×49 arcseconds with north at the top.

levels well below 90%. This suggests that preferential escape of ionizing radiation or long-term variability are indeed important in determining the ionization environment of AGN. Our data cannot yet distinguish which might have the dominant role, again parallel to studies of the Lyman α proximity effect.

4 CONCLUSIONS

Beginning with candidate pairs selected largely from the SDSS archive with the assistance of Galaxy Zoo volunteer participants, we have surveyed a sample of close companion galaxies to AGN for evidence of ionization of their interstellar medium by the external AGN. Such cases can help define the typical cone angles for escape of ionizing radiation, and the typical radiative history of AGN over timescales $\approx 10^5$ years. Chosen on the bases of predicted intensity of incident AGN radiation and fraction of solid angle covered by the companion, we observed 32 systems spectroscopically, of which 10 show spectroscopic evidence of AGN ionization in the companion galaxy or tidal structures. This compares reasonably well with our simple geometric estimate $\approx 18\%$, based on typical ionization cone opening angles 70° . A larger sample could, for example, place limits on rapid precession of ionization cones, if it were faster than the local recombination timescales. The distributions of predicted local ionizing flux from the AGN are similar in subsamples with and without evidence for cross-ionization, suggesting that the combination of geometric factors and variability history (instead of simply distance from the AGN and its luminosity) plays a key role in the AGN environment.

Further work in this direction could be pursued fruitfully with integral-field spectroscopy or narrowband emission-line imaging. Such data could define the regions within which AGN ionization is important. Emission-line imaging at high angular resolution would be more sensitive, allowing separation of the low-density diffuse ISM (whose ionization balance would be more easily altered by external radiation) from high-surface-brightness star-forming regions.

ACKNOWLEDGEMENTS

This work would not have been possible without the contributions of citizen scientists as part of the Galaxy Zoo project. Among the Galaxy Zoo volunteers, particularly extensive contributions were made by users zutopian and Blue_Crew. Other contributors to the sample compilation were Alice, Blackprojects, Budgieye, ElisabethB, Hanny van Arkel, Jean Tate, Kiske, LankyYankee, Lightbulb50, LynnSeguin, Ranny44, egalaxy, elizabeth, fatha731, graham d, joinpep, planetaryscience, and stellar190.

Galaxy Zoo was made possible by funding from a Jim Gray Research Fund from Microsoft and The Leverhulme Trust. We thank the Lick Observatory staff for their assistance in obtaining the data. VNB acknowledges assistance from National Science Foundation (NSF) Research at Undergraduate Institutions (RUI) grant AST-1312296. Findings and conclusions do not necessarily represent views of the NSF.

Funding for the creation and distribution of the SDSS Archive has been provided by the Alfred P. Sloan Foundation, the Participating Institutions, the National Aeronautics and Space Administration, the National Science Foundation, the U.S. Department of Energy, the Japanese Monbukagakusho, and the Max Planck Society. The SDSS Web site is <http://www.sdss.org/>. The SDSS is managed by the Astrophysical Research Consortium (ARC) for the Participating Institutions. The Participating Institutions are The University of Chicago, Fermilab, the Institute for Advanced Study, the Japan Participation Group, The Johns Hopkins University, Los Alamos National Laboratory, the Max-Planck-Institute for Astronomy (MPIA), the Max-Planck-Institute for Astrophysics (MPA), New Mexico State University, Princeton University, the United States Naval Observatory, and the University of Washington.

This research has made use of the NASA/IPAC Extragalactic Database (NED), which is operated by the Jet Propulsion Laboratory, Caltech, under contract with the National Aeronautics and Space Administration. The authors are honored to be permitted to conduct astronomical research on Iolkam Du'ag (Kitt Peak), a mountain with particular significance to the Tohono O'odham Nation.

REFERENCES

- Abazajian, K. N., Adelman-McCarthy, J. K., Agüeros, M. A., et al. 2009, *ApJS*, 182, 543-558
- Adelberger, K. L. 2004, *ApJ*, 612, 706
- Alam, S., Albareti, F. D., Allende Prieto, C., et al. 2015, *ApJS*, 219, 12
- Allen, M. G., Dopita, M. A., Tsvetanov, Z. I., & Sutherland, R. S. 1999, *ApJ* 511, 686
- Antonucci, R. 1993, *ARA&A* 31, 473
- Baldwin, J. A., Phillips, M. M., & Terlevich, R. 1981, *PASP* 93, 5
- Barth, A. J., Bentz, M. C., Greene, J. E., & Ho, L. C. 2008, *ApJL*, 683, L119
- Bianchi, S., Piconcelli, E., Pérez-Torres, M. Á., et al. 2013, *MNRAS*, 435, 2335
- Castro, C. S., Dors, O. L., Cardaci, M. V., & Hägele, G. F. 2017, *MNRAS*, 467, 1507
- Comerford, J. M., & Greene, J. E. 2014 *ApJL*, 789, 112
- Comerford, J. M., Barrows, R. S., Müller-Sánchez, F., et al. 2017, arXiv:1710.00825 (ApJ in press)
- Cutri, R. M., Wright, E. L., Conrow, T., et al. 2012, Explanatory Supplement to the WISE All-Sky Data Release Product, http://wise2.ipac.caltech.edu/docs/release/allsky/expsup/sec4_4h.html
- Elvis, M., Wilkes, B. J., McDowell, J. C., et al. 1994, *ApJS*, 95, 1
- Filippenko, A. V. 1982, *PASP* 94, 715
- Furlanetto, S. R., & Lidz, A. 2011, *ApJ*, 735, 117
- Gagne, J. P., Crenshaw, D. M., Kraemer, S. B., et al. 2014, *ApJ*, 792, 72
- Gonçalves, T. S., Steidel, C. C., & Pettini, M. 2008, *ApJ*, 676, 816
- Heckman, T. M., Bothun, G. D., Balick, B., & Smith, E. P. 1984, *AJ*, 89, 958
- Heckman, T. M., Kauffmann, G., Brinchmann, J., et al. 2004, *ApJ*, 613, 109

Hutchings, J. B., & Crampton, D. 1990, AJ, 99, 37

Keel, W. C., Kennicutt, R. C., Jr., Hummel, E., & van der Hulst, J. M. 1985, AJ, 90, 708

Keel, W. C., Kennicutt, R. C., Jr., van der Hulst, J. M., & Hummel, E. 1989, European Southern Observatory Conference and Workshop Proceedings, 32, 85

Keel, W. C., de Grijp, M. H. K., Miley, G. K., & Zheng, W. 1994, A&A, 283, 791

Keel, W. C. 1996, ApJS, 106, 27

Keel, W. C., Chojnowski, S. D., Bennert, V. N., et al. 2012, MNRAS 420, 878

Keel, W. C., Lintott, C. J., Schawinski, K., et al. 2012, AJ, 144, 66

Keel, W. C., Maksym, W. P., Bennert, V. N., et al. 2015, AJ 149, 155

Keel, W. C., Oswalt, T., Mack, P., et al. 2017, PASP, 129, 015002

Keel, W. C., Lintott, C. J., Maksym, W. P., et al. 2017, ApJ, 835, 256

Kennicutt, R. C., Jr., Roettiger, K. A., Keel, W. C., van der Hulst, J. M., & Hummel, E. 1987, AJ, 93, 1011

Kewley, L. J., Groves, B., Kauffmann, G., & Heckman, T. 2006, MNRAS, 372, 961

Kirkman, D., & Tytler, D. 2008, MNRAS, 391, 1457

Koss, M., Blecha, L., Mushotzky, R., et al. 2014, MNRAS, 445, 515

Lintott, C. J., et al. 2008, MNRAS, 389, 1179

Lintott, C. J., et al. 2009, MNRAS, 399, 129

Liu, X., Shen, Y., Strauss, M. A., & Hao, L. 2011, ApJ, 737, 101

Lipovetsky, V. A., Neizvestny, S. I., & Neizvestnaya, O. M. 1988, Soobshcheniya Spetsial'noj Astrofizicheskoy Obseruatorii, 55, 5

Miller, J.S. & Stone, R.P.S., Lick Obs. Technical Report 66 (Santa Cruz, CA: Lick Observatory)

Moran, E.C., Halpern, J.P., Bothun, G.D., & Becker, R.H. 1992, AJ 104, 990

Petrov, G. T., Kovachev, B. Z., & Mineva, V. A. 1985, ApSS, 116, 333

Sartori, L. F., Schawinski, K., Koss, M., et al. 2016, MNRAS, 457, 3629

Schawinski, K., Evans, D. A., Virani, S., et al. 2010, ApJL 724, L30

Schawinski, K., Koss, M., Berney, S., & Sartori, L. F. 2015, MNRAS, 451, 2517

Schirber, M., Miralda-Escudé, J., & McDonald, P. 2004, ApJ, 610, 105

Schirmer, M., Diaz, R., Holhjem, K., Levenson, N. A., & Winge, C. 2013, AJ, 763, 60

Schmitt, H. R., Donley, J. L., Antonucci, R. R. J., et al. 2003, ApJ, 597, 768

Schweizer, F., Seitzer, P., Kelson, D. D., Villanueva, E. V., & Walth, G. L. 2013, AJ, 773, 148

Secrest, N. J., Schmitt, H. R., Blecha, L., Rothberg, B., & Fischer, J. 2017, ApJ, 836, 183

Stockton, A., Fu, H., & Canalizo, G. 2006, NewARv 50, 694

Storchi-Bergmann, T., Schmitt, H. R., Calzetti, D., & Kinney, A. L. 1998, AJ, 115, 909

Veilleux, S., Shopbell, P. L., & Miller, S. T. 2001, AJ, 121, 198

Visbal, E., & Croft, R. A. C. 2008, ApJ, 674, 660

Wehrle, A. E., & Morris, M. 1988, AJ, 95, 1689

Wilson, A. S. 1996, Vistas in Astronomy, 40, 63

Wright, E. L., Eisenhardt, P. R. M., Mainzer, A. K., et al. 2010, AJ, 140, 1868

APPENDIX A: SOURCE LIST: LOW REDSHIFT AGN/COMPANION GALAXY PAIRS

For completeness, tableA1 gives relevant properties of all 212 AGN/galaxy pairs considered. Selection properties were projected angle subtended by the companion galaxy around the AGN (θ) and predicted ionizing flux from the AGN at the projected distance of the companion galaxy (F_{ion}). F_{ion} was estimated as in Section 2.1, using the [O III] $\lambda 5007$ fluxes calculated, where possible, from the SDSS spectra (based on tabulated line equivalent width EW in Å and local continuum flux F_{cont} , as tabulated in SDSS DR7). Objects are identified both by coordinate designation, with initial J indicating designations used in the Sloan surveys (Alam et al. 2015); and, for SDSS objects, by the Data Release 12 (Alam et al. 2015) numerical ObjID for ease of data retrieval. For compactness, F_{cont} is listed in units 10^{-17} erg cm $^{-2}$ s $^{-1}$ Å $^{-1}$. F_{ion} is given in arbitrary units, since the quantity has systematic uncertainties as well as projection effects and was used only to rank objects for spectroscopic observation.

In a few cases we used additional sources for emission-line data: Petrov et al. (1985) for NGC 6786, Heckman et al. (1984) for the companion of PG 1048+342, and Keel et al. (1985) for NGC 5278/9.

“Type” indicates the AGN type - 1 for broad-line objects (as in Sy 1), 2 for narrow-line objects, and 0 for BL Lac objects.

Table A1. Source list.

Coord ID	SDSS ObjID	Type	$z(\text{AGN})$	$z(\text{compn})$	r''	θ°	F_{cont}	EW	F_{ion}	Notes
J001707.95+011506.2	1237678617419710603	2	0.1057	0.1074	11	40	19.90	32.10	22	
J002228.37-005830.6	1237657189833900309	1.5	0.1060	0.1060	12	70	9.00	25.80	6.8	
J002944.89+001011.1	1237663784200634427	2	0.0598	0.0594	5	30	28.7	114.3	552	
J005754.03+012013.8	1237678617424166953	2	0.0567		9	30	325	402	6800	UM 293
J011309.59+021716.5	1237680100234887247	1.9	0.0462		72	28				UGC 768
J011448.67-002946.0	1237666338653012001	1	0.0338	0.0349	17	45	52.00	12.90	9.8	UGC 793
J011659.06+001933.3	123766633972015947	1	0.0782	0.0077	9	55	19.20	2.80	2.8	
J013037.75+131252.0	1237649918432116906	2	0.0722	0.0726	16	100	14.00	23.30	5.4	
J020436.76-115943.4	1237676674463826080	1.5	0.0726		24	45				
J021209.23+072127.5	1237670016730333231	2	0.1424		6	45	4.20	5.00	2.5	
J022226.11-085701.3	1237652900226596935	1	0.1666		3	70	15.20	106.60	759	
J022909.70+010043.0	1237678617434128461	2	0.1283	0.1288	8	30	8.60	11.60	6.6	
J024222.87-011009.0	1237660024521556048	2	0.0372	0.0376	23	20	17.20	17.80	2.4	
J025445.35+010308.4	1237678437018108063	2	0.1367	0.1366	9	20	8.70	7.40	3.3	
J025740.83-163046.0	1237667244870008884	1	0.0679		5	80				
J030858.44-001549.0	1237660240312467582	2	0.2064	0.2069	3	80	5.50	80.00	206	
J033213.20+001546.7	1237666301093675376	1	0.0861	0.0875	8	100	26.40	6.80	11.8	
J072612.51+412233.7	1237673706650796616	1	0.1324		4	70	11.50	6.30	19.1	
J073402.62+433236.9	1237663916261703871	1	0.0831	0.0823	8	45	23.00	15.00	23	
J073906.17+442409.9	1237663915725357374	2	0.1345	0.1408	4	80	12.50	4.10	13.5	
J074408.20+435935.6	1237663530254663877	2	0.1331	0.1348	5	70	7.00	9.00	10.6	
J074429.85+284721.9	1237657119477989769	2	0.1015	0.1025	4	110	12.00	10.30	33	
J074547.87+265537.9	1237657630578376999	1.8	0.1148		8	40	29.00	88.10	168	
J075433.27+204635.2	1237661087490441736	1.8	0.1146	0.1146	8	50	8.00	40.00	21	
J075648.78+501016.6	1237663915728175471	1	0.2366	0.2364	6	45	9.00	13.60	14.3	
J075729.04+351105.9	1237654626788704563	2	0.1117		3	110	16.1	14.1	106	
J080059.77+343412.0	1237674290219450784	2	0.0823	0.0811	8	40	20.00	22.60	30	
J080435.27+363711.5	1237654652024390067	2	0.0913		11	40	15.00	22.80	11.9	
J080514.10+364942.9	1237654652024521006	2	0.0841		16	20	14.00	11.60	2.7	
J080647.76+282512.8	1237658192145744217	2	0.1426		8	75	10.70	6.80	4.8	
J081411.26+144735.4	1237667253453521141	2	0.1572		9	30	9.50	10.88	5.4	
J082017.99+465125.3	1237651250946244661	2	0.0524		8	50	12.00	29.00	23	
J082034.78+153111.2	1237667253454241925	1	0.1438		8	90	14.30	6.50	6.1	
J082913.59+264009.9	1237661087494766877	2	0.0574	0.0571	18	20	26.00	50.00	16.9	
J083049.39+102712.5	1237671262269997354	2	0.0727	0.0720	17	33	18.20	24.20	6.4	
J083116.14+351707.4	1237657629510271237	1.9	0.1601		3	90	10.00	53.20	249	
J083202.71+093759.1	1237671261196255490	2	0.0750		4	130	21.00	10.20	56	
J083224.28+355135.9	1237657775539945655	2	0.1368		6	60	15.00	14.30	25	
J083728.08+391723.7	1237657401878708344	2	0.1147		20	30	17.50	41.80	7.7	
J083848.14+040734.0	1237658423540580569	2	0.0476	0.0484	9	20	72.00	39.70	149	
J083902.96+470756.3	1237654381974716589	2	0.0524	0.0534	18	20	38	71	36	
J084135.08+010156.2	1237650797286850905	2	0.1106		4	80	19.2	400.1	2020	
J084742.44+344504.4	1237658191076720756	1	0.0640	0.0653	22	30	850	3.1	97	PG 0844+349
J084810.11+351534.3	1237664871356891234	2	0.0573	0.0570	4	80	19.5	33.2	170	
J085152.62+522833.0	1237651190821617882	1	0.0645		11	70	14.00	20.40	9.9	
J085820.50+642048.4	1237663917882802416	1	0.1158		5	30	11.50	59.70	116	
J090128.46+352030.1	1237664871894941906	2	0.1053		7	40	30.10	46.90	121	
J090134.48+180943.0	1237667429554585733	2	0.0665	0.0665	9	40	32.00	14.90	25	
J090317.39+100100.5	1237661069779009763	2	0.0619		12	130	31.12	24.10	22	UGC 4748
J090436.92+553602.9	1237651252024836118	1	0.0372		12	75	80.0	32.3	76	
J090604.60+170120.0	1237667485918429442	2	0.1007		8	45	15.00	52.80	52	
J090743.49+013327.9	1237660670347706621	1	0.1643		5	75	18.70	6.90	22	
J090810.33+500923.1	1237654653642801161	1	0.0981	0.1073	13	50	44.00	23.80	26	
J091029.08+203401.9	1237667210510336112	2	0.0289	0.0280	25	270	75.00	11.40	5.8	
J091141.65+370204.1	1237660635988492309	1	0.0865	0.0862	14	30	30.00	39.20	25	
J091319.00+532958.4	1237654383052062933	1.9	0.2549		3	20	13.00	9.30	57	
J091449.05+085321.1	1237660670347706621	1	0.1399		3	75	10.10	6.90	33	
J091540.88+155639.7	1237667735026532578	2	0.1434		9	40	11.00	35.00	20	
J091930.42+133258.7	1237671125373485313	1	0.2291	0.2297	8	120	55.00	9.40	34	
J093044.15+084929.7	1237661064413249768	2	0.1304	0.1300	4	40	11.00	108.40	314	
J093811.95+045356.5	1237658298454180052	1.8	0.1626		4	180	12.00	10.20	32	
094542.04-141934.8		2	0.0077	0.0081	87	20				NGC 2992
J094716.12+534944.8	1237655108368597025	2	0.0383		15	90	16.20	47.60	14.4	

Table A1 – continued Source list

Coord ID	SDSS ObjID	Type	z (AGN)	z (compn)	r''	θ°	F_{cont}	EW	F_{ion}	Notes
J094741.58+633939.2	1237651540315930774	2	0.1390		3	50	16.00	12.40	93	
J095847.90+144526.2	1237671261742694538	2	0.0767		7	60	15.50	10.10	13.5	
J095958.22+030232.7	1237654599952760951	2	0.0907	0.0906	17	40	20.00	44.70	13.0	
J100531.67+183939.0	1237667782284017791	2	0.0779	0.0780	7	70	14.00	10.90	13.1	
J100534.70+392852.8	1237660772882907153	1	0.1408		12	25	22.00	9.00	5.8	
J100602.50+071131.8	1237658300604743843	2	0.1205	0.1218	5	80	25.00	80.50	339	
J101043.36+061201.4	1237658423550607494	1	0.0978		4	20	39.3	116.1	1200	
J101202.59+301303.0	1237665097393963129	1	0.0498		12	70	55.00	49.60	80	
J101439.55-004951.2	1237654669200326683	2	0.0491	0.0483	19	20	41.00	13.20	6.3	UGC 5528
J101653.82+002857.0	1237654670811201558	2	0.1163		2	50	20.90	191.70	4220	
J101932.86-032014.9	1237650803195248686	1	0.0500	0.0492	37	35				Mkn 1253
J102027.52+135530.1	1237661070861140238	2	0.1449		6	15	16.00	21.40	40	
J102250.45+495936.5	1237657858213871668	2	0.1155		16	55	11.70	9.70	1.9	
J102536.43+371317.1	1237664669509550195	2	0.0608		5	180	34.00	7.00	40	
J102850.92+163917.9	1237671262819713088	2	0.1720		5	75	5.40	16.80	15.3	
J102940.71+015555.1	1237651753463578759	2	0.0412	0.0418	40	50	37.50	38.00	3.8	UGC 5694
J103000.93+085202.6	1237660583909720086	2	0.0522		20	35	63.00	12.00	8.0	
J103011.81+035410.7	1237654604787745026	2	0.0510		11	50	22.00	11.20	8.6	
J103216.14+505120.0	1237657589242396682	1	0.1737		3	120	22.40	16.10	169	
J103600.37+013653.5	1237651752927363244	2	0.1068		7	25	42.00	105.90	382	
J103607.13+191048.1	1237667781213421682	2	0.1117		10	70	14.00	7.30	4.3	
J103655.60+380321.4	1237662226206228529	2	0.0507	0.0500	29	40	48.60	23.20	5.6	
J103734.22+140120.5	1237661070326104198	2	0.2060		5	20	23.00	46.00	178	
J103819.51+161445.1	1237671261746888940	2	0.1359		3	35	13.00	14.70	89	
J103825.16-002331.1	1237654669739819119	2	0.0963		4	180	14.00	4.50	16.6	
J104232.05+050241.9	1237654602104897626	2	0.0272	0.0273	9	180	26.0	19.4	26	NGC 3341
J104519.45+123839.3	1237661068179406916	2	0.0394	0.0398	8	60	45.00	14.50	43	
J105030.47+232931.4	1237667538012602552	1.8	0.0604		5	50	18	19.2	58	
J105128.41+335850.8	1237665129609691296	1	0.1828		5	55	9.00	17.30	26	
J105143.89+335926.7	1237665129609756690	1	0.1671	0.1670	4	40	81.00	17.30	369	PG 1048+342
J105203.60+060349.4	1237658422481387583	1.8	0.1281	0.1285	11	15	18.00	9.00	5.6	
J105222.48+180711.1	1237668288550076449	1	0.1322		2	120	26.00	17.00	466	
J105418.31+181344.7	1237668288550273059	2	0.0811		10	30	16.00	20.90	14.1	
J105434.78+302211.7	1237665329844322346	2	0.1055		13	20	16.00	15.50	6.2	
J105503.48+425136.8	1237661850925793371	2	0.0592	0.0590	11	50	35.00	22.40	27	
J105505.07+414944.8	1237661871322955907	2	0.1077		2	120	8.20	17.30	149	
J105521.02+291849.3	1237667212668895318	2	0.1408		3	30	6.50	40.00	122	
J105738.07+082007.5	1237671930135445716	2	0.0371	0.0366	26	60	15.00	7.90	0.7	
J110017.99+100256.8	1237671932283322446	2	0.0360	0.0361	20	170	40.00	17.10	7.2	UGC 6081
J110157.90+101739.3	1237658493883711561	1.5	0.0341	0.0347	31	80	48.3	198.5	42	Tol 1059+105
J110301.26+120543.0	1237661950246322306	2	0.1184		6	45	16.00	22.40	42	
J110427.30+381232.2	1237662224597909569	0	0.0302	0.0313	12	20				Mkn 421
J110525.11+215229.6	1237667783364051073	2	0.1475		4	80	11.80	93.00	289	
J110544.44+195746.3	1237668294982500461	2	0.1043		4	90	16.00	13.00	55	
J110550.53+205113.3	1237667734501326907	2	0.1015		8	25	22.00	26.70	39	
J110612.16+061347.6	1237658422482895003	2	0.0979	0.0986	17	20	12.00	23.20	4.1	
J110639.11+433620.9	1237661872934682808	2	0.1185	0.1186	5	110	23.40	5.40	21	
J110816.45+293210.5	12376677255082745989	2	0.0466	0.0467	9	60	25.00	12.50	16	
J111118.04+352308.3	1237664817671438525	2	0.0250		9	45	45.00	14.10	33	
J111159.48+013643.4	1237651752931360818	1.9	0.1108	0.1099	7	30	13.00	25.80	29	
J111154.61+065143.2	1237661971178586191	1	0.1492		9	25	12.00	85.30	53	
J111623.16+532413.3	1237657589782413395	2	0.1123	0.1125	2	100	17.00	6.10	109	
J111943.34+451612.6	1237661852538568731	2	0.2036	0.2030	6	60	10.00	323.60	379	
J112336.17+521810.0	1237657857681260680	2	0.1579		11	30	12.00	32.50	13.6	
J112353.48+655133.5	1237651537636032650	2	0.1326		7	50	8.80	10.90	8.2	
J112525.71+533344.4	123765800960700483	2	0.0804	0.0808	17	50	26.00	18.30	6.9	
J112602.45+343448.1	1237665025437139019	1.5	0.1113	0.1115	11	140	21.00	27.90	20	
J112949.25+172020.2	1237668585971253453	1	0.1571		4	45	12.00	41.60	132	
J113003.10+655629.3	1237651271361495049	1	0.1326		4	90	19.60	26.80	138	
J113215.11+244516.8	12376677550885314686	1	0.1711		4	50	7.40	6.60	12.9	
J113240.25+525701.3	1237657630599872600	2	0.0266	0.0271	34	30	180	71.4	47	Mkn 176
J113321.04+373944.3	1237664819821019315	2	0.1754		6	30	7.90	10.30	9.5	
J113323.97+550415.8	1237658802571968533	1	0.0085	0.0078	8	> 120	1.30	11.90	1.0	Mkn 177

Table A1 – continued Source list

Coord ID	SDSS ObjID	Type	$z(\text{AGN})$	$z(\text{compn})$	r''	θ°	F_{cont}	EW	F_{ion}	Notes
J113342.78+353135.4	1237665026511601678	1	0.2018	0.2036	4	90	31.00	29.50	241	
J113443.24+153848.0	1237661070869069974	2	0.0698	0.0693	12	50	30.00	30.80	27	
J113800.25+482623.2	1237658611445530792	1	0.1000	0.1002	4	120	15.00	24.50	97	
J113858.89+141253.2	1237664289924055180	2	0.0805		8	75	22.6	67.3	100	
J113942.52+315433.7	1237665368509710424	1.5	0.0089	0.0090	84	30	50.00	1.00		NGC 3786
J114154.76+465656.9	1237660635464466499	2	0.0728		4	90	1.60	12.40	5.2	
J114252.83+325124.2	1237665369583779929	2	0.0666	0.0661	15	40	27	101.8	51	
J114719.94+075243.1	1237661972255736072	2	0.0826	0.0821	15	30	27.00	28.90	14.6	
J115112.99+064105.9	1237661970645581860	1	0.0768	0.0807	13	80	25.00	15.30	9.5	
J115535.35+125253.9	1237661813346009111	1	0.1216		8	25	57.00	5.20	19.5	
J120041.39+314746.2	1237665226229940236	2	0.1159		4	55	80	400	8530	
J120149.74-015327.5	1237650762390765695	1	0.0907		5	50	18.0	147.2	8426	
J120235.97+372157.8	1237664818749767887	2	0.1975		6	75	12.00	18.40	26	
J120336.87+200629.2	1237668298202415270	2	0.2121		3	90	11.40	209.00	1115	
J120349.20+020556.9	1237651753473867953	1.5	0.0812		8	40	23.50	10.90	17	
J120655.62+501737.4	1237658205047488538	1.5	0.0621	0.0633	50	35	35.50	22.90	1.4	
J120712.57+165809.6	1237668623548022885	2	0.0723	0.0737	13	85	24.00	6.51	3.9	
J120836.75+223934.3	1237667782833602610	1	0.1997		3	90	18.30	8.90	76	
J121015.67+262837.4	1237667441896390838	2	0.1041		8	20	38.00	37.00	93	
J121151.12+443327.6	1237661850395017428	2	0.1003		15	120	16.00	11.00	3.3	
J121155.63+372113.4	1237664818750619663	2	0.0838	0.0834	8	90	14.00	41.30	38	
J121303.35+513855.2	1237657855537053802	2	0.0849		7	100	22.0	42.6	81	
J121418.25+293146.7	1237667253478424610	2	0.0632	0.0640	7	100	31.	58.5	156	Was 49
J121522.77+414620.9	1237661966355988618	1	0.1963		5	45	17.00	99.10	284	
J121749.78+354449.6	1237665025978663019	2	0.0881	0.0880	4	120	14.00	10.30	38	
J121943.13+132659.9	1237661813885436022	2	0.0647	0.0645	11	110	25	71	62	
J121953.10+554506.8	1237658918529925220	1	0.1075		11	25	19.50	70.90	48	
J122026.09+044631.9	1237655125009498294	2	0.0811	0.0803	45	12	8.00	200.00	3.3	
J122157.16+080515.1	1237661972259537090	2	0.0718		12	45	30.20	47.60	42	
J122500.80+014401.8	1237651752939290772	2	0.0897	0.0898	25	45	28.00	20	3.8	
J122744.56-015140.2	1237650371558703219	1	0.1484		5	40	22.60	22.60	86	
J123152.05+450443.1	1237661872941367322	1	0.0622	0.0621	20	60	55.00	12.00	7.0	
J123351.61+195311.6	1237667915421778099	2	0.0737	0.0735	7	50	15.00	12.10	16	
J123507.49+171509	1237668589724631143	2	0.0894	0.0898	11	40	19.30	26.00	17	
J124214.47+141147.0	1237662524694462694	2	0.1574		15	20	14.00	17.60	4.6	
J124322.55+373858.0	1237664819290177687	2	0.0859	0.0865	6	90	37	17.3	74	
J124406.59+652925.5	1237654610679955615	2	0.1071		4	75	21.50	129.00	730	
J130116.09-032829.0	1237650369414889508	2	0.0864	0.0867	11	70	34.80	24.90	30	
J130240.41+514644.4	1237661958293028932	2	0.0539	0.0550	110	12	28.20	57.70	0.6	UGC 8151
J130354.71-030631.8	1237650760786903297	2	0.0778		6	60	36.2	38.6	163	
J130600.68+000125.0	1237648704582844527	2	0.1379	0.1377	13	20	11.00	94.60	26	
J131135.65+142447.1	1237662525234479221	1	0.1140		9	45	60.00	42.10	131	
J131318.92+504001.7	1237661957220139201	2	0.1585		6	55	13.20	26.10	40	
J131517.26+442425.5	1237661851473739819	2	0.0355	0.0355	37	90	110.00	27.20	9.2	
J131639.74+445235.0	1237661852010676264	2	0.0906	0.0915	12	25	45.00	166.50	219	
J131854.19+221825.5	1237667783377551471	2	0.1818		3	90	8.20	11.60	45	
J132751.63+330638.1	1237665127476428926	2	0.1412		2	70	13.70	13.60	196	
J133920.85+393224.3	1237662305112293614	2	0.2240		3	90	39.00	200.00	3650	
J134143.75+554025.5	1237661387065786478	2	0.0251	0.0253	38	45	3100.00	15.00	136	NGC 5278/9
J134203.48+183901.5	1237668271899738298	1.8	0.0845		5	80	17.6	134.4	399	
J134234.31+191338.9	1237668272436674636	1	0.0866	0.0866	9	180	49.00	11.10	28	
J134730.70+603743.1	1237655369829580934	1	0.1433	0.1438	5	30	15.20	25.40	65	
J134736.39+173404.6	1237668316456288331	2	0.0447	0.0451	10	90	40	51.9	87	
J134955.48+084039.6	1237662236939256056	2	0.0670		10	30	220.00	6.80	63	
J135255.67+252859.6	1237665531709554737	1	0.0636		5	60	40.00	40.70	274	
J135429.05+132757.2	1237662529526890706	2	0.0633		9	60	8.4	420	183	
J135713.88+115951.0	1237662199886184522	2	0.0205	0.0205	85	30	97.30	4.60	0.3	
J14044.19+100429.7	1237662239088836793	2	0.0958	0.0951	26	12	12.40	30.40	2.3	
J141041.49+223337.0	1237667911678099640	1	0.1725		3	35	31.50	43.00	634	
J141104.81-001906.6	123764870453051635	2	0.1387	0.1390	5	60	11.50	16.00	31	
J141447.15-000013.1	1237648721245503521	2	0.0475	0.0474	5	70	24.0	28.8	116	
J141946.07+650353.2	1237674479196242084	1	0.1479		4	70	25.00	50.00	329	

Table A1 – *continued* Source list

Coord ID	SDSS ObjID	Type	z (AGN)	z (compn)	r''	θ°	F_{cont}	EW	F_{ion}	Notes
J142255.49-001711.4	1237648704054362331	2	0.1302		5	40	5.00	200.00	168	
J142755.36-003341.8	1237648720710074546	2	0.0795	0.0792	7	50	15.00	22	29	
J142802.22+062619.5	1237655744015368412	2	0.1155		13	45	8.90	18.80	4.2	
J143454.21+334934.5	1237662661597659257	2	0.0578	0.0587	14	35	30.00	5.4	3.5	
J143515.65+023221.6	1237651754564190252	1	0.3048		6	25	46.70	15.10	82	
J144213.96+231844.6	1237665532251406538	1	0.1830		9	30	6.10	5.90	1.9	
J144248.27+120040.3	1237662529532133399	0	0.1631		2	120	42.00	0.40	18	
J144733.17-013844.3	1237655499209310386	2	0.0428	0.0427	73	26	28.70	3.90	0.1	
J144937.71+184159.5	1237667783386988590	2	0.0321	0.0320	29	45	89.40	3.00	1.3	
J145002.97+255441.2	1237665178450788549	1.8	0.0604		7	60	15.00	15.80	20.4	
J145051.51+050652.1	1237651822714028249	2	0.0275	0.0282	21	55	100.00	76.40	73	NGC 5765
174659.8 +683637		1	0.0630	0.0623	7	120				Kaz 163
182205.11+663719.2		2	0.0155	0.0146	24	150				Kaz 199 NGC 6636
191152.98+731929.5		2	0.0250	0.0252	85	10				NGC 6786
J220041.34+103308.0	1237678859532566564	2	0.0266		3	120				Mkn 520
J220555.01-000755.2	1237663543146643720	2	0.0945	0.0939	13	60	13.30	4.40	1.5	
J220701.98+101400.8	1237678876177072140	2	0.0266	0.0266	13	75				NGC 7212
J225057.27-085410.8	1237652600111366327	1.8	0.0650	0.0644	6	30	35.00	23.50	96.3	
J225452.22+004631.3	1237663445442691192	1	0.0909	0.0912	11	40	57.50	7.70	15.4	
J225823.29+001603.8	1237663444906213507	2	0.1542	0.1543	10	45	16.10	5.30	3.6	
J230315.61+085226.0	1237679034548551752	1	0.0163	0.0160	71	50	0.00		0.0	NGC 7469
J230443.47-084108.6	1237653438155128872	1	0.0470	0.0473	63	13	172.00	109.80	20	Mkn 926
J232756.70+084644.3	1237679034014367754	2	0.0289	0.0295	45	80				NGC 7674
J234428.33+010829.7	1237656909037699193	2	0.1206	0.1167	11	40	13.90	19.60	9.5	